Kinetics of Solid-State Reactions in Al-Li-Cu-Mg-Zr Alloys from Calorimetric Studies

K.S. GHOSH, K. DAS, and U.K. CHATTERJEE

Differential scanning calorimetric (DSC) studies at different heating rates have been carried out to examine the solid-state reactions in 1441 and 8090 Al-Li-Cu-Mg-Zr alloys of water-quenched (WQ) and retrogressed tempers. The DSC peaks indicating the reactions sequence such as formation of GPB zones, precipitations of δ' phase, dissolution of GPB zones and δ' precipitates, and precipitations of S', T_1, T_2, and δ phases have been identified. From the heat flow associated with the peaks of the thermograms, the fraction transformation (Y), the rate of transformation (dY/dt), the activation energy (Q^*), the frequency factor (k_0), and the transformation function $f(Y)$ for all the reactions of the 1441 and 8090 alloys have been determined. The appearance of separate peaks of GPB zone formation and δ' precipitation in the 1441 alloy of retrogressed tempers has enabled determination of the kinetic parameters, which is otherwise not possible from the thermograms of the WQ state due to peak overlapping, by varying heating rate method. The kinetic parameters determined from the DSC data of all the reactions of the alloys are in good agreement with the previously published data.

DOI: 10.1007/s11661-007-9250-2

I. INTRODUCTION

THE attractive combination of Al-Li alloys of 5 to 10 pct decrease in density, 15 to 25 pct increase in elastic modulus, and 10 to 15 pct increase in specific strength over the widely used 2xxx and 7xxx aluminum alloys has rendered them as candidate materials for aerospace applications.[1–7] However, Al-Li alloys have unattractive fracture behavior, especially poor ductility and toughness arising due to the inhomogeneous nature of slip resulting from matrix strengthening ordered δ' (Al_3Li) and coarse equilibrium δ (AlLi) grain boundary precipitates.[1,3,6,7] Al-Li alloys are also susceptible to environment-induced cracking (EIC).[8] In commercial pentanary Al-Li-Cu-Mg-Zr alloys, slip is homogenized by introducing dispersoids β' (Al_3Zr) and semicoherent/incoherent precipitates of T_1 (Al_2CuLi), θ' (Al_2Cu), or S (Al_2CuMg) phases, with the additions of Zr, Cu, and Mg.[1,6,7] A large number of metastable precipitate phases that occur in the alloys and the wide variety of aging treatments employed can lead to complex microstructural conditions. Thus, a good description of the microstructure is essential to the understanding of structure-property relationships. The microstructural changes that occur in these alloys upon aging and retrogression and reaging treatment have been examined by a number of investigators.[1,6,7,9,10]

For a rapid and quantitative description of solid-state phase transformations, differential scanning calorimetry (DSC) study is considered as a supplement to transmission electron microscopy (TEM) studies.[11,12] The kinetics of precipitation and dissolution reactions in aluminum-base alloys have been analyzed by various researchers using resistivity measurements and the DSC technique.[13–18]

The retrogression and reaging (RRA) treatment applicable to precipitation hardenable aluminum alloys has been studied in detail to assess microstructural changes,[3,7,19] mechanical properties.[20] and EIC.[21–23] However, the DSC studies of the retrogressed and RRA tempers are scanty. In the present work, the kinetics of the precipitation and dissolution reactions of 1441 (Russian grade) and 8090 Al-Li-Cu-Mg-Zr alloys have been studied from the DSC data, and the significance of retrogression treatment that enabled determination of the kinetic parameters for the overlapping peaks of the water-quenched (WQ) states has also been discussed.

II. EXPERIMENTAL PROCEDURES

A. *Materials*

The DSC studies were carried out on the 1441 and 8090 Al-Li-Cu-Mg-Zr alloys. The compositions of the alloys are given in Table I. The alloys were obtained in sheet form from the Defence Metallurgical Research Laboratory (DMRL), Hyderabad, India. The 1441 and 8090 alloys were cast, homogenized, hot rolled, and cold rolled to a thickness of 2.0 and 2.8 mm, respectively. The cold-rolled sheet of the 1441 alloy was solutionized at 530 °C to 535 °C, WQ, stretched by 1.5 to 2.5 pct, followed by low-high duplex artificial aging at 150 °C for 4 hours and

K.S. GHOSH, Assistant Professor, is with the Department of Metallurgical and Materials Engineering, National Institute of Technology, Warangal 506 004, India. Contact e-mail: ksghosh2001@yahoo.co.uk K. DAS, Associate Professor, and U.K. CHATTERJEE, Emeritus Professor, are with the Department of Metallurgical and Materials Engineering, Indian Institute of Technology, Kharagpur 721 302, India.

Manuscript submitted September 19, 2006.
Article published online August 4, 2007.

Table I. Chemical Compositions (Weight Percent) of the 8090 and 1441 Al-Li-Cu-Mg-Zr Alloys

Alloy	Li	Cu	Mg	Zr	Fe	Si	Al
1441	1.90	2.0	0.90	0.09	0.11	0.05	balance
8090	2.29	1.24	0.82	0.12	0.09	0.044	balance

then 170 °C for 24 hours to the peak-aged T8 temper. However, the 8090 alloy sheet was solutionized at 530 °C to 535 °C, WQ, stretched 1.5 to 2.5 pct, followed by artificial aging at 170 °C for 24 hours to the peak-aged T8 temper. The T8 temper alloy sheets were subjected to retrogression treatments above the δ' solvus line, followed by immediate cooling in ice-cold water. The T8 temper of the 1441 alloy was retrogressed at 230 °C for 15 minutes and at 270 °C for 5 minutes, whereas the T8 temper of the 8090 alloy was retrogressed at 250 °C for 12 minutes and at 280 °C for 8 minutes.[3,7,20]

B. *DSC Runs and Baseline Correction*

The DSC runs to the 1441 and 8090 alloys of solution-treated and WQ and retrogressed tempers were initiated in an argon atmosphere from ambient temperature to 540 °C at different heating rates of 5 °C/min, 10 °C/min, 15 °C/min, and 20 °C/min, using a Stanton Redcroft (PL Thermal Sciences & Rheometric Scientific Thermal Analysers, Surrey, UK) model STA 625 (heat flux type) simultaneous thermal analyzer. Specimens of approximately 30 mg were cut from the coupons of the various tempers of both the alloys. The sides of the specimens were made absolutely flat and smooth for very good contact with the crucible.

In the DSC studies, baseline and baseline drift are properly accounted for in measuring accurate and reliable calorimetry heat evolution and absorption, because no instrument is perfect and free from parasitic effects, although modern DSC instruments are reliable and show remarkably high accuracies in measurements. The STA system used for DSC studies was purged with argon gas for half an hour before starting the experiment. The STA thermal analyzer was connected to a computer with a suitable interface; the data for each run was continuously stored. After a run was completed, the output, *i.e.*, the net heat flow as a function of temperature was recorded using the established calibration of the DSC cell. Baseline calibration runs on annealed pure aluminum as well as on the standard sapphire sample were made. The baseline and sapphire data were used to generate a "look-up" table. Further, calibration run on an ICTA temperature standard, *e.g.*, indium, was stored in the default data area of the computer, where the experimental run data were also stored. During subsequent experiments, this table was used to convert the raw data counts to rate of heat transfer. The output, the net heat flow, to the reference (high-purity annealed aluminum) relative to the samples was recorded as a function of temperature. At least two runs were made for each sample in order to establish reproducibility. The procedure for analysis of DSC data for determining kinetic parameters is discussed in Section III.

III. RESULTS AND DISCUSSION

A. *Identification of DSC Peaks*

Figures 1 and 2 show the DSC curves of the 1441 and 8090 alloys of solution-treated and WQ states at heating rates of 2.5 °C/min, 5 °C/min, 10 °C/min, and 20 °C/min, respectively. The thermograms of the alloys of WQ state and annealed pure aluminum, at the heating rate of 10 °C/min, are also shown separately within the insets. In the case of age-hardenable aluminum alloys, nor-

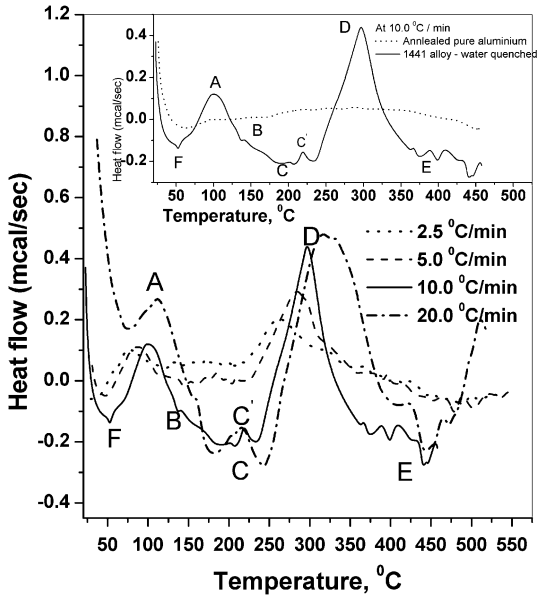

Fig. 1—DSC thermograms of the solution-treated and WQ 1441 alloy at different heating rates. Thermograms within the subset are for the alloy and annealed pure aluminum at 10 °C/min.

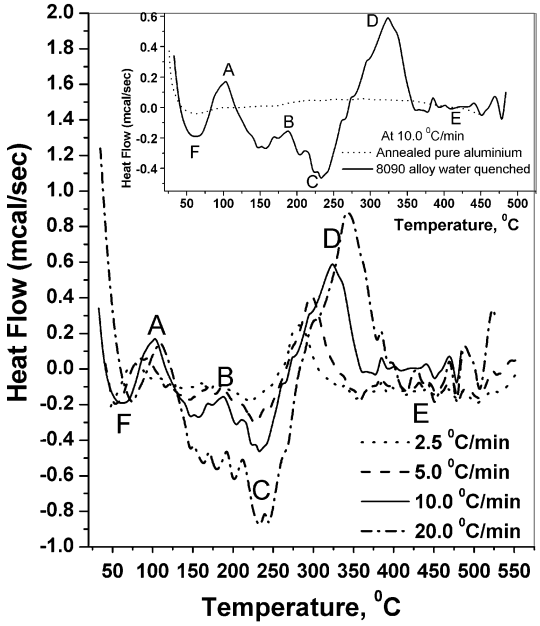

Fig. 2—DSC thermograms of the solution-treated and WQ 8090 alloy at different heating rates. Thermograms within the subset are for the alloy and annealed pure aluminum at 10 °C/min.

mally, the formation of precipitates is an exothermic process while their dissolution is an endothermic process.[24] The peak temperature for the precipitation represents the temperature at which the two factors, *i.e.*, the fall of the driving forces for the continued precipitation (*i.e.*, the decrease of supersaturation with the rise of temperature during DSC run) and the increase of diffusivity with the increase of temperature compete and result in a maximum precipitation rate. The exothermic and endothermic peaks in Figures 1 and 2 are marked with A through F, which indicate the sequence of precipitation and dissolution reactions occurring in the alloys. The peaks are identified as follows: A—formation of GPB zones, B—precipitation of δ' (Al_3Li) phase, C—dissolution of GPB zones and δ' precipitates, D—precipitation of S', T_1, T_2, and δ phases, E—dissolution of S', T_1, T_2, and δ phases, and F—dissolution of Li-bearing zones. The identification of the peak regions and temperatures is consistent with the literature.[18,25–28]

B. *Analysis of DSC Data*

In the DSC run, the total heat effects, $Q(T)$, observed between the initial temperature of a peak T_i and at a temperature T are given by

$$Q(T) = \frac{EA(T)}{M\phi} \quad [1]$$

where M is the mass of the sample; ϕ is the heating rate; E is the (calibration) constant; and $A(T)$ is the area under the peak between temperatures T_i and T, which is the observed heat flow that is associated with the precipitation and dissolution reactions. The $A(T)$ term can be expressed as

$$A(T) = \int_{T_i}^{T} (\delta q) dT \quad [2]$$

where δq is the measured heat flow, involved for the specific precipitation or dissolution reactions, to the inert reference (high-purity annealed aluminum) relative to the sample as a function of temperature at a constant heating rate ϕ.

If T_f is the final temperature of the peak,

$$Q(T_f) = \frac{EA(T_f)}{M\phi} \quad [3]$$

If Q_0 is the heat effect per mole of precipitate, then the heat effect dQ is given by

$$dQ = Q_o dn \quad [4]$$

where dn in the number of moles of precipitate that form or dissolve per unit mass of the alloy.

Integrating Eq. [4] [yields $Q(T) = Q_o\ n(T)$] and putting in Eq. [1], we obtain

$$n(T) = \frac{EA(T)}{Q_0 M\phi} \quad [5]$$

and

$$n(T_f) = \frac{EA(T_f)}{Q_0 M\phi} \quad [6]$$

Thus, the mole fraction of the precipitation, $Y(T)$, at temperature T, can be expressed as

$$Y(T) = \frac{n(T)}{n(T_f)} \quad [7]$$

Therefore, from Eqs. [5] through [7],

$$Y(T) = \frac{A(T)}{A(T_f)} \quad [8]$$

From the DSC thermograms, the fraction transformed $Y(T)$, *i.e.*, the amounts of phase precipitated or dissolved at a given temperature range, can be expressed according to Eq. [8] and is illustrated schematically in Figure 3.

The rate of transformation can be written

$$\frac{dY}{dt} = \frac{dY}{dT} \cdot \frac{dT}{dt}$$

Thus,

$$\frac{dY}{dt} = \frac{dY}{dT} \cdot \phi \quad [9]$$

C. *Kinetic Parameters of Solid-State Reactions in the 1441 and 8090 Alloys*

1. *1441 alloy: peak A—GPB zones and δ' phase*

Figure 1, the thermogram of the 1441 alloy, at low temperature, shows only the peak A region. The peak B

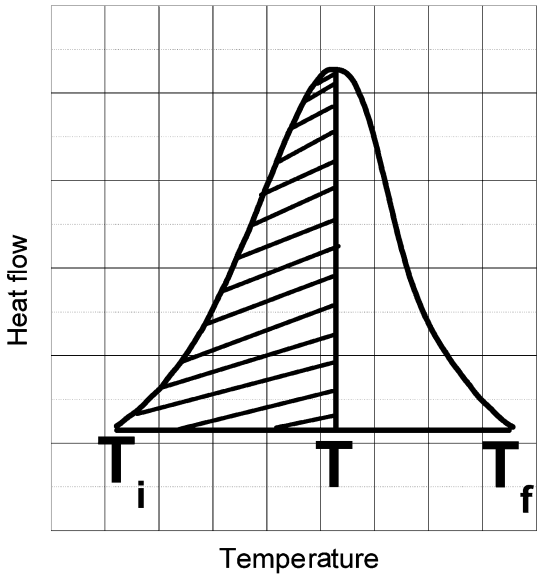

Fig. 3—Shaded area showing the fraction transformation within the temperature range T_i to T_f.

region (usually the temperature range for the precipitation of δ' phase in the Al-Li alloy system) has not been resolved clearly with a sharp peak; instead, a small thermal fluctuation is observed. This suggests that the δ' phase has precipitated at some other temperature, preferably at lower temperature; otherwise, the question arises, how the strength properties are met in the alloy. Thus, the peak region A is considered to be a purely compound one comprising overlapping peaks for the formation of GPB zones and precipitation of δ' phase. Because the Li content is less in the 1441 alloy, the δ' solvus line is lowered by about 20 °C with respect to that in the 8090 alloy, as estimated from the Al-Li phase diagram.[29] Further, the presence of higher amounts of Cu and Mg in the 1441 alloy (compared with the 8090 alloy) decreases Li solubility in Al, which favors both the precipitation and growth of δ' particles, mostly in the first stages of aging. All of these effects cause δ' precipitation in the 1441 alloy at a lower temperature, with respect to that in the 8090 alloy, resulting in overlapping of peak B with peak A. So, the determination of activation energy from the peak region A of Figure 1 will not be accurate and representative either for the formation of GPB zones or for the precipitations of δ' phase.

Figures 4(a) through (c), DSC thermograms of the retrogressed states, exhibit separate peak regions A and B and represent the formation of GPB zones and δ' phase precipitation at different temperatures, respectively. This will enable accurate determination of the kinetic parameters for either of the reactions. Noble and Trowsdale[30] also employed a slow quench to produce the δ' peak plus one precursor peak in Al-10 at. pct Li alloy, so that the thermal events were sufficiently well separated to enable consistent activation energy to be measured, as they observed overlapping peaks in rapidly quenched alloy.

2. *Precipitation of δ' phase in the 1441 alloy of retrogressed tempers*

Figures 4(a) and (b), the DSC thermograms of the 1441R2300 and 1441R270 retrogressed tempers of the 1441 alloy at a heating rate 10 °C/min, exhibit two clearly distinct exothermic peaks, A (formation of GPB zones) and B (precipitation of δ' phase), compared to the overlapping compound peak A for the WQ state (Figure 1). This is because of the differences in concentrations of solutes in the retrogressed and WQ states. In the retrogressed temper, the solid solution is supersaturated largely with Li atoms and with small amounts of Cu and Mg, as retrogression treatment of the T8 temper has caused dissolution primarily of δ' and partially of S' and T_1 phases, confirmed in the literature.[3,7,19,20] However, in the as-quenched state, the solid solution is fully supersaturated with the entire contents of solutes Cu, Li, and Mg. Thus, the retrogressed tempers, being supersaturated largely with Li atoms in the presence of small amounts of Cu and Mg in the solid solution, require higher thermal energy for the precipitation of δ' phase as compared to that required for the WQ state. Hence, during the DSC run, the precipitation of δ' in the

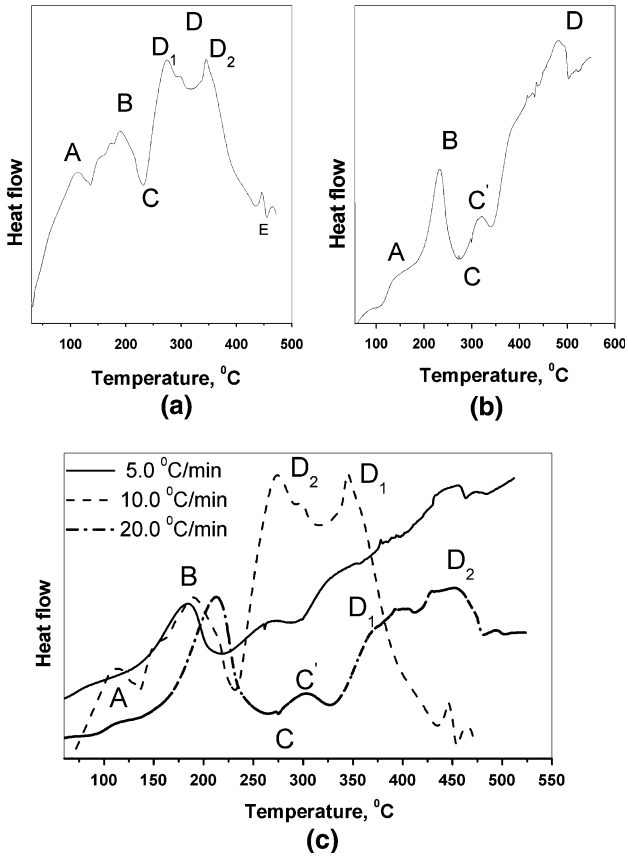

Fig. 4—DSC thermograms of the (*a*) 1441R230 and (*b*) 1441R270 retrogressed tempers at the heating rate of 10 °C/min and (*c*) 1441R230 temper at different heating rates.

retrogressed tempers has occurred at a higher temperature compared to that in the as-quenched state.

The peak B of the 1441R230 retrogressed state at different heating rates is shown in Figure 5(a). From these curves, the precipitate amount (mole fraction, Y) and precipitate rate (dY/dt) can be calculated after Eqs. [8] and [9] and are shown as a function of temperature in Figures 5(b) and (c), respectively. The Y *vs* T curves for the δ' precipitations in the 1441 alloy are sigmoidal in shape and the curves have shifted to higher temperatures with the increase in heating rates. There are also considerable shifts in the maxima of the rate of transformation curves (Figure 5(c)) to the higher temperatures with the increase in heating rates, implying that the precipitation process is thermally activated and kinetically controlled.

For nonisothermal reactions, the kinetic parameters can be determined using Eq. [10], which is also described in the literature:[18]

$$\ln\,[(dY/dT)\,\phi] = \ln[f(Y)k_0] - (Q^*/R)\,(1/T) \quad [10]$$

where k_0 is the frequency factor, $f(Y)$ is a function of Y only, Q^* is the activation energy, R is the gas constant, T is the absolute temperature, and (dY/dT) is obtained from Y *vs* T curves (Figure 5(b)). The activation energy (Q^*) of the process can be determined by

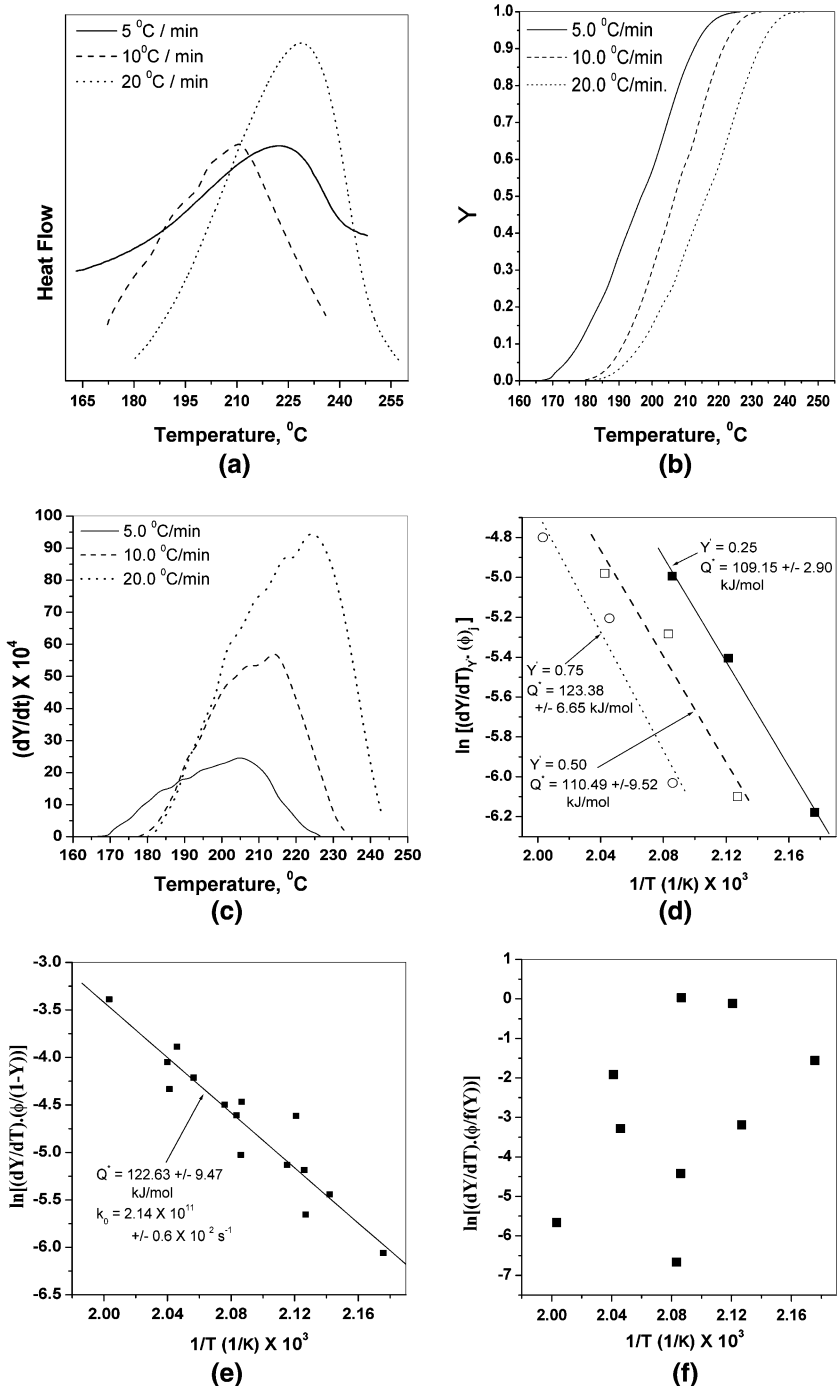

Fig. 5—(*a*) The δ' phase precipitation of the retrogressed 1441R230 state at different heating rates. (*b*) *Y vs T* plots of δ' phase precipitation of the 1441R230 retrogressed temper. (*c*) Plot of $(dY/dt) \times 10^4$ *vs T* of the peak region *B* of the 1441R230 temper. (*d*) Plot for the determination of activation energy for δ' precipitation in the 1441R230 temper after Eq. [11]. (*e*) Plot after Eq. [16] for determination of $f(Y)$ for the peak region *B* of 1441R230 retrogressed temper. (*f*) Plot after Eq. [15] if $f(Y) = [1 - (1 - Y)^{1/3}]^2$ for the peak region B of the 1441R230 temper.

varying heating rate method; if, for a heating rate ϕ_j, the temperature at which a constant mole fraction (Y') of precipitate obtained is T_j, then

$$\ln[(dY/dT)_{Y'}\phi_j] = \ln[f(Y')k_0] - (Q^*/\mathrm{R})(1T_j) \qquad [11]$$

where ϕ_j is the *j*th heating rate, $(dY/dT)_Y$is the rate at a given mole fraction (Y'), and T_j is the temperature at which the mole fraction is (Y') at heating rate ϕ_j. Therefore, a plot of $\ln\ [(dY/dT)_{Y'}\phi_j]$ *vs* $(1/T_j)$, under different heating rates, will give a straight line of slope $(-Q^*/R)$ from which the value of activation energy, Q^*, can be determined.

The data obtained from Figures 5(a) through (c) are plotted after Eq. [11] in Figure 5(d) for three values of mole fraction transformed, Y' (0.25, 0.50, and 0.75). The slopes of the three linear straight lines give the average

Table II. Kinetic Parameters for Solid-State Reactions in the 1441 and 8090 Alloys

Alloy	Peak Nature of the Peak	A GPB Zone Formation	B δ' Precipitation	C δ' Dissolution	D S' Precipitation	F Li-Bearing Dissolution
1441	Q^* (kJ/mol) (Eq. [11])	—	114.34 ± 6.65	—	75.46 ± 7.09	38.79 ± 5.85
	Q^* (kJ/mol) (Eq. [16])	—	122.50 ± 9.48	132.19 ± 4.16	70.99 ± 5.03	—
	k_0 (s^{-1})		$2.14 \times 10^{11} \pm 0.6 \times 10^2$	$1.16 \times 10^{12} \pm 2.88$	$3.21 \times 10^4 \pm 2.69$	
	$f(Y)$		$(1 - Y)$	$(1 - Y)$	$(1 - Y)$	
8090	Q^* (kJ/mol) (Eq. [11])	68.42 ± 5.70	—	137.33 ± 8.58	77.67 ± 2.87	40.25 ± 6.40
	Q^* (kJ/mol) (Eq. [16])	71.99 ± 3.07	—	143.58 ± 9.31	87.78 ± 4.5	—
	k_0 (s^{-1})	$1.44 \times 10^8 \pm 2.75$		$8.84 \times 10^{12} \pm 9.33$	$4.42 \times 10^5 \pm 2.77$	
	$f(Y)$	$(1 - Y)$		$(1 - Y)$	$(1 - Y)$	

activation energy, which is found to be about 114.34 ± 6.65 kJ/mol.

To describe the progress of reactions at all temperatures and for all temperature-time programs, the function $f(Y)$, the constants k_0 and Q^* need to be determined. In general, the reaction function $f(Y)$ is unknown at the outset of the analysis. A range of standard functions, which represent particular idealized reaction models, have been proposed.[31,32] The function $f(Y)$ is determined by assuming suitable forms and using experimental data to verify. Reactions that occur by nucleation and growth yield sigmoidal behavior. A general relationship[33] that gives sigmoidal behavior is

$$f(Y) = Y^r(1 - Y)^m \quad [12]$$

where exponents r and m are constant. The formalism can incorporate Johnson–Mehl–Avrami–Kolmogorov (JMAK) kinetics and the forms that also yield sigmoidal behavior are

$$f(Y) = n[-\ln\ (1 - Y)]^{(n-1)/n}(1 - Y) \quad [13]$$

where the exponent n, growth parameter, is a constant that depends on the precipitate growth modes. If n is considered to be unity, Eq. [13] reduces to

$$f(Y) = (1 - Y) \quad [14]$$

Further, for a three-dimensional diffusional equation, the transformation function $f(Y)$ may also be expressed as[15]

$$f(Y) = [1 - (1 - Y)^{1/3}]2 \quad [15]$$

Plots are made to verify the validity of the preceding expressions for the precipitation of δ' phase. However, the relationship in Eq. [14] is most satisfactory, as shown in Figure 5(e), whereas the other relationship after Eq. [15] is unsatisfactory, as shown in Figure 5(f). Combining Eqs. [9], [10], and [14] yields

$$\ln\left[(dY/dT)\left(\frac{\phi}{1 - Y}\right)\right] = \ln k_0 - \left(\frac{Q^*}{\mathrm{R}}\right)\left(\frac{1}{T}\right) \quad [16]$$

The activation energy for the δ' precipitation in the 1441R230 retrogressed temper after Eq. [16] is found to be 122.50 ± 9.48 kJ/mol and k_0 is found to be $2.14 \times 10^{11} \pm 0.6 \times 10^2\ s^{-1}$. The activation energies, Q^*, obtained after Eqs. [16] and [11] are in close match. Thus, the transformation function for the precipitation of δ' phase in the 1441 alloy is $f(Y) = (1 - Y)$. The kinetic parameters and transformation functions obtained from the DSC data for all the precipitation and dissolution reactions occurring in the 1441 and 8090 alloys are given in Table II.

In the preset work, the activation energy for the δ' precipitation in the 1441 alloy determined from the retrogressed state is higher than the value 86 kJ/mol reported by Noble *et al.*[30] and 84 kJ/mol reported by Luo *et al.*[18] The activation energy for diffusion of lithium in aluminum is 130 to 140 kJ/mol, but for the movement of vacancies in aluminum, it is in the range of 41 to 67 kJ/mol.[31–33] So, our present observation is in agreement with the data for diffusion of lithium in aluminum. It is therefore likely that the excess vacancies will be present at or near the regions forming δ' and thus increase the diffusivity of lithium in aluminum to the growing precipitate.

In the present work, the average activation energy of 114 to 122 kJ/mol for the precipitation of δ' phase reveals that the precipitation is predominantly associated with the diffusion of lithium in aluminum, and the movement of vacancies in aluminum assisting the formation of δ' precipitates in the retrogressed state is marginal. This is because the excess vacancy level is quite low in the retrogressed state, as the retrogressed state (and, further, the peak-aged temper is subjected to retrogression treatment) is quenched only from 230 °C to 270 °C, whereas the solution-treated water state is generally quenched from high-temperature 530 °C to 540 °C.

Peak A in Figure 1 is a compound one and represents the formation of GPB zones and the precipitation of δ' phase. Therefore, the determination of activation energy after Eq. [11] by the varying heating rate method will not be accurate and representative for either of the reactions. Further, it is also not possible to do so after Eq. [11] from peak A of the DSC thermograms of the retrogressed tempers (Figures 4(a) through (c)), because peak A is not well developed in all the heating rates.

3. *8090 alloy: peak A—GPB zones*

The kinetic parameters for peak A of GPB zone formation in 8090 alloy can be determined after Eq. [11],

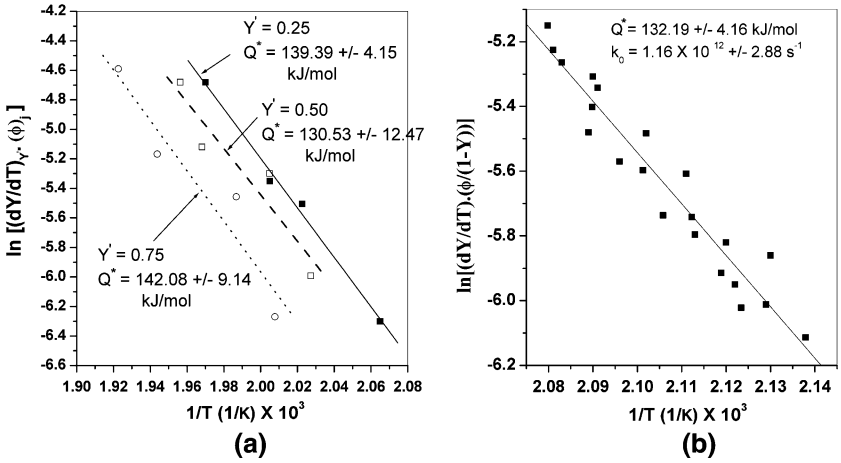

Fig. 6—(*a*) Plot for the determination of activation energy for the dissolution of GPB zones and δ' precipitates of the 8090 alloy after Eq. [11]. (*b*) Determination of activation energy after Eqs. [18] and [16] for the dissolution of GPB zones and δ' phase of the 1441 alloy.

and the average activation energy value was found to be 68.42 ± 5.70 kJ/mol. The activation energy value is in good agreement with the value obtained by others.[14,18] The obtained activation value is also consistent with the value expected for the formation of GPB zones in the presence of excess quenched-in vacancies generated upon quenching from solutioning temperature (530 °C). The migration energy of vacancies in Al-Cu, Al-Li alloys has been reported to be in the range of 41 to 69 kJ/mol.[30,34,35]

Further, the activation energy, Q^*, for the formation of GPB zones determined after Eq. [16] has been found to be 71.99 ± 3.07 kJ/mol, which is excellent agreement with the value obtained after Eq. [11]. The frequency factor, k_0, value is found to be $1.44 \times 10^8 \pm 2.75\ s^{-1}$. In this method of calculating the activation energy after Eq. [16], the growth parameter, n, is taken as unity. Generally, n may be an integer or a fraction and depends on the precipitate growth modes *i.e.*, spherical rods or discs.[36] The GPB zones have been reported to be cylindrical in shape.[37] If the growth of the cylindrical particles occurs by diffusion control, the radius of the zone will be proportional to $\sqrt{t}$ and the function $f(Y)$ will be $(1 - Y)$;[38] hence, this transformation function is considered to be consistent.

The calculated activation energy, Q^*, has to be taken as the apparent activation energy, because the process involved is not unique and also not precisely definable. In fact, the peak A region should be considered as a compound one, involving the formation of GPB zones and precipitation of δ' phase, as the latter one also commences from the room temperature itself. However, the formation of GPB zones is the dominant reaction in this peak A region; thus, the calculated activation energy can be taken as reasonably accurate and representative for the GPB zone formation. The determination of kinetic parameters for the GPB zones in the aluminum alloys is also likewise reported in the literature.[14,18,26]

4. *Peak C—dissolution of δ' precipitates and GPB zones in the 1441 and 8090 alloys*

The peak region C is identified for the dissolution of δ' precipitates and GPB zones. The kinetic parameters for the dissolution of δ' phase and GPB zones in the 8090 alloy are calculated from peak C using the varying heating rate method, after Eqs. [8], [9], and [11]. Figure 6(a) shows the plot of the logarithm of $[(\frac{dY}{dT}) \cdot \phi_j]$ *vs* $\frac{1}{T_j}$ for peak C, and the activation energy Q^* is found to be 137.33 ± 8.58 kJ/mol. The term Q^* obtained after Eq. [16] is found to be 143.58 ± 9.31 kJ/mol. Thus, the function of δ' phase dissolution can be expressed as $f(Y) = (1 - Y)$. The k_0 is found to be $8.84 \times 10^{12} \pm 9.33\ s^{-1}$. The activation energy determined in the present work for the δ' phase dissolution is in good agreement with the value 131.5 kJ/mol for δ' dissolution in binary Al-Li alloy and 128.50 ± 3.5 kJ/mol for Al-Li-Cu-Mg-Zr alloy reported in the literature.[17,18] Because the obtained activation energy value lies around 120 to 140 kJ/mol, the dissolution of δ' precipitates in 8090 alloy is believed to be associated with the diffusion of lithium in aluminum.

In the peak region C of Figures 1 and 2, thermal fluctuation or even doublets have been observed. This thermal fluctuation phenomenon is so prominent for the 1441 alloy that a distinct exothermic peak C′ is exhibited. A similar observation has also been reported in the literature for Al-Li as well as in other Al-base alloys.[717] The existence of a distinct exothermic peak C′ in the peak region C is the net effect of the commencement of exothermic precipitation reactions and the endothermic dissolution process of δ' precipitates. The appearance of the exothermic C′ peak in the peak region C indicates that exothermic precipitation reactions have dominated over the dissolution reactions of δ' precipitates.

Beyond the temperature of the C′ peak, the thermograms showing heat flow again in the endothermic direction indicate the ongoing continued dissolution of δ' precipitates, especially which are larger in size,

pinned, and engulfed with β' dispersoids.[7,17] A similar exothermic C′ peak has also appeared in retrogressed 1441R230 and 1441R270 tempers as well, as shown in Figures 4(b) and (c). Therefore, unless some corrections and modifications are incorporated for calculating the fraction dissolution after Eq. [8], it is difficult to determine accurately the fraction dissolution Y and activation energy for the dissolution of δ' precipitates of the 1441 alloy in the peak region C from the thermograms of the WQ (Figure 1) and retrogressed tempers (Figure 4(c)) as well.

Jena *et al.*[14] stated that, under the situation of overlapping peaks, the total area under the peak region of contention could be estimated by considering and doubling the area of the overlapping region. Thus, the total area $A_1(T_f)$ for the dissolution process in the peak region C should be estimated by considering the double of the area (say, A_2) of the C′ peak, and adding this with the area in the peak region C, $A(T_f)$, without considering the C′ peak. Thus,

$$A_1(T_f) = A(T_f) + 2A_2 \qquad [17]$$

Therefore, Eq. [8] becomes modified as

$$Y(T) = \frac{A(T)}{A_1(T_f)} \qquad [18]$$

The kinetic parameters for the dissolution of δ' precipitates and GPB zones in the 1441 alloy are calculated from the peak region C, after Eqs. [18] and [16], and the plot of $\ln\left[(dY/dT)\left(\frac{\phi}{1-Y}\right)\right]$ *vs* $\frac{1}{T}$ is shown in Figure 6(b). The activation energy and k_0 for peak C in 1441 alloy are found to be 132.19 ± 4.16 kJ/mol and $1.16 \times 10^{12} \pm 2.88\ s^{-1}$, respectively. The Q^* is in good agreement with the reported value 128.5 ± 3.5 kJ/mol for the dissolution of δ' precipitates and GPB zones.[24,25]

5. *Peak D: precipitations of S′ and T_1 phases in 1441 and 8090 alloys*

The peak region D in Figures 1 and 2 is associated with the precipitation of S' (S), T_1, T_2, and δ phases.[25,26,39,40] Luo *et al.*[18] observed that the heat effects observed in this peak region for the 8090 alloy are close to twice that of GPB zones and δ' precipitation and suggested that the peak D represents both S' and δ phases. Gupta *et al.*[10] have proposed that S' is only a slightly strained version of S, and the heat effects associated with the $S' \rightarrow S$ transformation will be minimal and the DSC trace is unlikely to exhibit a separate peak. Mukhopadhyay *et al.*[24] stated that, over the range of the exothermic peak, the S-phase precipitation exotherm also overlaps with the precipitation of δ phase. Miller *et al.*[6] found the coprecipitation of S' phase with T_1 and δ phases in the microstructure of 8090-T8 alloy. The relative amounts of these phases are difficult to estimate and are critically dependent on the relative concentrations of the alloying elements. However, in the 8090 type alloy, the S' phase is predominantly more than the T_1 phase and also is in relatively much higher proportions compared with the T_2 and δ phase. Although the peak D region is associated with precipitation of S' (S), T_1, T_2, and δ phases, the relative amounts of T_2 and δ phases are less in the DSC thermograms of the WQ state of the alloys compared to those of the T8 and retrogressed and reaged (RRA) tempers. In fact, authors[3,7] have observed a wider peak D for the DSC thermograms of the T8 and RRA tempers of the 8090 alloy, and in fact, for the T8 and RRA tempers of the 1441 alloy, with two distinct peak regions D_1 and D_2 as compared to that of a sharp peak region D of the WQ state. Therefore, the kinetic parameters determined from the DSC thermograms from the WQ states are mostly for the precipitations of S' and T_1 phases, which is also mentioned in the literature.[25]

The exothermic DSC peak D of the WQ 1441 alloy at different heating rates is shown in Figure 7(a). The fraction of precipitation Y and the precipitation rate (dY/dt) with temperature calculated after Eqs. [8] and [9] are shown in Figures 7(b) and (c), respectively. The Y *vs* T curves (Figure 7(b)) are typically sigmoidal in shape and shifted to higher temperatures with the increase in heating rates. There are also considerable shifts in the maxima of the rate of transformation curves (Figure 7(c)) to the higher temperatures with the increase in heating rates, and this implies the transformation is thermally activated and kinetically controlled. Figure 7(d) shows the plot for determining the activation energy, Q^*, after Eq. [11], and the average activation energy is found to be 75.46 ± 7.09 kJ/mol. Similarly, the activation energy determined after Eq. [11] for the peak region D in the 8090 alloy is found to be 77.67 ± 2.87 kJ/mol.

The activation energies of the exothermic peak D of the 1441 (shown in Figures 7(e)) and 8090 alloys also determined after Eq. [16] are found to be 70.99 ± 5.03 and 87.78 ± 4.5 kJ/mol, respectively, which are also in an excellent agreement with those obtained after Eq. [11]. The frequency factors, k_0 values for the 1441 and 8090 alloys, are found to be $3.21 \times 10^4 \pm 2.69\ s^{-1}$ and $4.42 \times 10^5 \pm 2.77\ s^{-1}$, respectively. Hence, the transformation function that best describes the precipitation of S' phase in the alloys is $f(Y) = (1 - Y)$. This agrees with the reaction function for the formation of rod-shaped S'-phase precipitates suggested in the literature,[14,38] either by diffusion-controlled parabolic growth or diffusion-controlled linear axial growth, which is expected to satisfy the Johnson–Mehl type expression where the value of the coefficient n is equal to one. Plot is also made to verify the validity of the transformation function for the precipitation of S′ phase after Eq. [15], but the relationship is unsatisfactory, as shown in Fig. 7(f).

6. *Peak F dissolution of Li-bearing zones*

The appearance of an endothermic peak F at low temperature in Figures 1 and 2 represents the dissolution of Li-bearing zones, *i.e.*, the Li-lean regions, or even ordered Li-rich regions that still had to develop onto stoichiometric δ' (Al_3Li) composition.[36,41] The formation of Li-bearing zones[10,40] is attributed to the fact

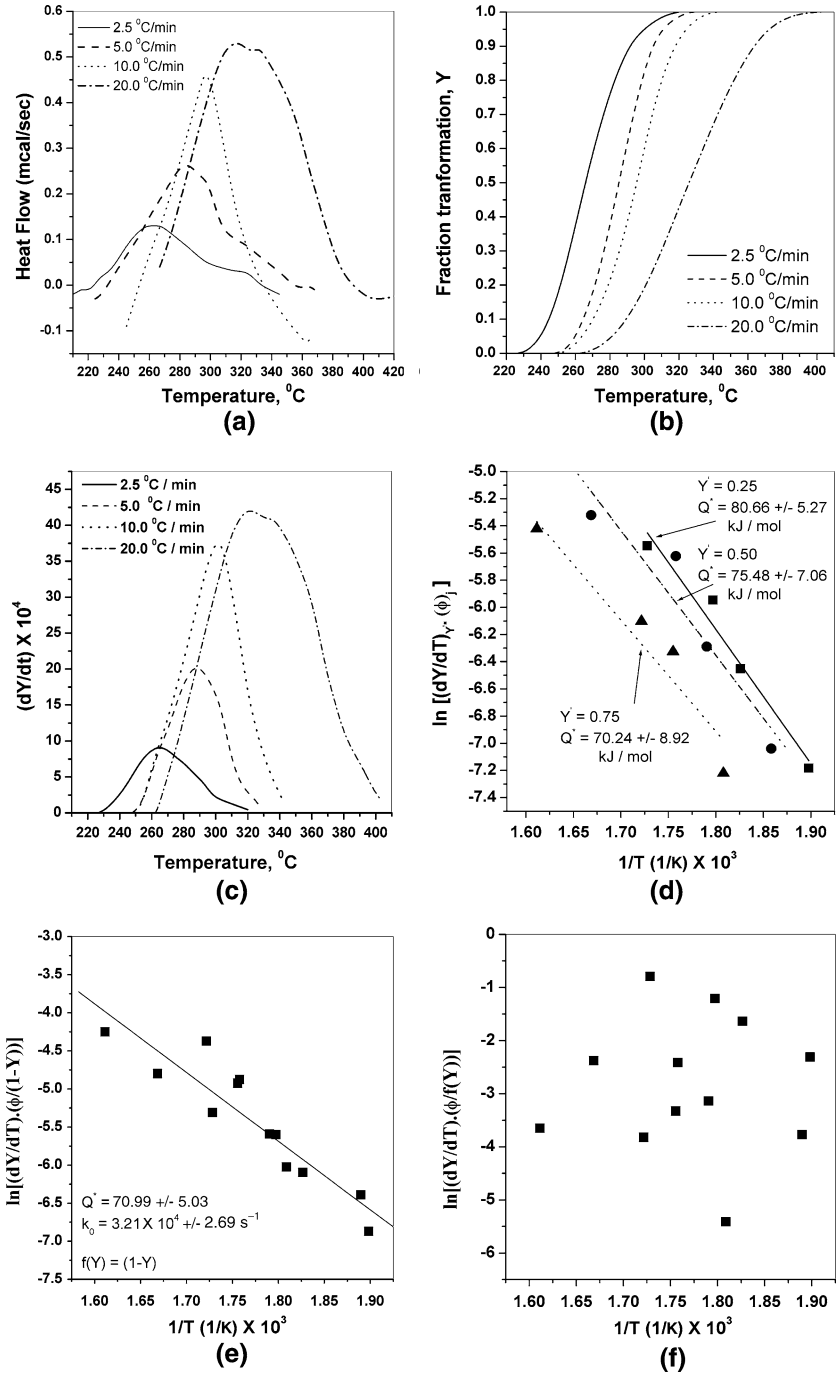

Fig. 7—(*a*) The *S*′ phase precipitation peaks in the solution-treated and WQ 1441 alloy at different heating rates. (*b*) *Y vs T* plots of peak D of solution-treated WQ 1441 alloy. (*c*) Plot of $(dY/dt) \times 10^4$ *vs T* of the peak region D of the 1441 alloy. (*d*) Plot for the determination of the activation energy for the peak region D of the 1441 alloy after Eq. [11]. (*e*) Plot after Eq. [16] for determination of $f(Y)$ for the peak region D of the 1441 alloy. (*f*) Plot after Eq. [15], if $f(Y) = [1 - (1 - Y)^{1/3}]^2$ for the peak region D of the 1441 alloy.

that, upon quenching the alloys from the solution treatment temperature, excess vacancies are quenched-in; this is because the Li-vacancy binding energy is high in the Al-Li and in the ternary Al-Li-Zn system.[42] Noble *et al.*[30] believed it was caused by dissolution of subcritical $L1_2$ ordered regions. Sato *et al.*[43] invoked a similar interpretation to explain the observed low-temperature endotherm in their DSC studies of as-quenched Al-Li alloys. Further, Rio *et al.*[44] detected the formation of ordered regions of size less than 1 nm in Al-10 at. pct Li alloy, aged for 24 hours at room temperature, by the positron annihilation technique, and reported these regions dissolved on heating when δ' grew.

The peak region F (Figures 1 and 2) also indicates that the peak minima have shifted to higher temperatures with the increase of heating rates. The kinetic parameters are determined for the dissolution of

Li-bearing zones in the similar manner as described in the previous sections. The activation energy Q^* values obtained after Eq. [11] for the 1441 and 8090 alloys are found to be 38.79 ± 5.85 kJ/mol and 40.25 ± 6.40 kJ/mol, respectively, indicating that the excess vacancies formed upon quenching assist the dissolution process. The activation energy values for the dissolution of a similar type of peak reported by Luo *et al.*[18] and Noble *et al.*[30] in binary Al-Li alloy are 58.5 and 70 kJ/mol, which are higher than in our observation. This difference could be explained considering the excess vacancies level. They have reported the calculation of activation energy from the state of WQ and naturally aged at room temperature for 24 hours, whereas in our calculation, it is from the WQ state only.

IV. CONCLUSIONS

1. The DSC thermograms of solution-treated and WQ 1441 and 8090 alloys, at different heating rates, exhibit many exothermic and endothermic peaks, which indicate the sequence of precipitation and dissolution reactions such as the formation of GPB zones, precipitation of δ' phase, dissolution of GPB zones and δ' phase, precipitation of S', T_1, T_2, and δ phases, *etc*. The shifting of all the reaction peaks at higher temperatures with increasing heating rates implies that the reactions are thermally activated and kinetically controlled processes.
2. From the DSC data, the method to determine fractional transformation (Y), activation energy (Q^*), frequency factor (k_0), and the function $f(Y)$, of the rate equation have been discussed.
3. Thermograms of the WQ state in the 1441 alloy showing overlapping peaks of GPB zones and δ' precipitation will not yield in determining kinetic parameters accurately for either of the reactions by the varying heating rate technique. However, thermograms of the retrogressed state exhibiting separate peaks of GPB zone formation and δ' precipitation enable determination of kinetics parameters. The Q^*, k_0, and $f(Y)$ of δ' precipitation in the 1441 alloy determined from the retrogressed state are 122.50 ± 9.48 kJ/mol, $2.14 \times 10^{11} \pm 0.6 \times 10^2$ s^{-1}, and $(1 - Y)$, respectively. The δ' precipitation is believed to be associated predominantly with the diffusion of lithium in aluminum.
4. The activation energy Q^*, frequency factor k_0, and the function $f(Y)$ of the rate equation for the formation of GPB zones in the 8090 alloy are 68.42 ± 5.70 kJ/mol, $1.44 \times 10^8 \pm 2.75$ s^{-1} and $(1 - Y)$, respectively. Thus, the GPB zone formation is by quenched-in vacancies assisted by diffusion of solutes.
5. The dissolution of δ' precipitates in the 1441 and 8090 alloys has occurred in the temperature range of 162 °C to 275 °C at all the heating rates. The Q^*, k_0, and $f(Y)$ for the δ' dissolution in the 1441 and 8090 alloys are 132.19 ± 4.16 kJ/mol, $1.16 \times 10^{12} \pm 2.28$ s^{-1}, and $(1 - Y)$ and 143.58 ± 9.31 kJ/mol, $8.84 \times 10^{12} \pm 9.33$ s^{-1}, and $(1 - Y)$, respectively. The dissolution of δ' precipitates is suggested as the diffusion-controlled process.
6. The activation energies of S' phase in the 1441 and 8090 alloys are found to be 70.99 ± 5.03 and 87.78 ± 4.5 kJ/mol, respectively. The transformation function that best describes the precipitation of S' phase is $(1 - Y)$. This suggests that the rod-shaped S' phase precipitates form either by diffusion-controlled parabolic growth or diffusion-controlled linear axial growth, which is expected to satisfy the Johnson–Mehl type expression, where the value of the coefficient n is equal to one.
7. Li-bearing zones, which form during quenching of the alloys, dissolve at low temperature upon subsequent aging. The activation energy for the dissolution of Li-bearing zones in the 1441 and 8090 alloys are found to be 38.79 ± 5.85 kJ/mol and 40.25 ± 6.40 kJ/mol, respectively, indicating that the excess vacancies formed upon quenching assist the dissolution process.

ACKNOWLEDGMENTS

The authors thank Drs. A.A. Gokhale and Vijaya Singh, Scientist, Defence Metallurgical Research Laboratory (DMRL), Hyderabad, India, for providing the alloys. Thanks are due to Mr. Nirmal Das, Central Research Facility, IIT – Kharagpur, India, for his assistance in carrying out DSC runs.

REFERENCES

1. *ASM Specialty Handbook: Aluminum Lithium Alloys*, J.R. Davis ed., International Materials Information Society, Materials Park, OH, 1998, pp. 121–42.
2. E.J. Lavernia, T.S. Srivatsan, and F.A. Mohamed: *J. Mater. Sci.*, 1990, vol. 25, pp. 1137–58.
3. K.S. Ghosh, K. Das, and U.K. Chatterjee: *Metall. Mater. Trans. A*, 2004, vol. 35A, pp. 3681–91.
4. P.J. Gregson and H.M. Flower: *Proc. Int. Conf. on Aluminium Technology '86*, T. Sheppard, ed., The Institute of Metals, London, 1986, pp. 423–28.
5. A.F. Smith: *Aluminium-Lithium Alloys*, Proc. 4th Int. Al-Li Conf., G. Champier, B. Dubost, D. Miannay, and L. Sabetay, eds., *J. Phys.*, Paris, Suppl. 1987, vol. 48, p. C3:49.
6. W.S. Miller, J. White, and D.J. Lloyd: *Aluminium-Lithium Alloys*, Proc. 4th Int. Al-Li Conf., G. Champier, B. Dubost, D. Miannay, and L. Sabetay, eds.; *J. Phys.*, Paris, Suppl. 1987, vol. 48, p. C3:139.
7. K.S. Ghosh, K. Das, and U.K. Chatterjee: *Mater. Sci. Technol.*, 2004, vol. 20, pp. 825–34.
8. A. Gray: *Aluminium-Lithium Alloys*, Proc. 4th Int. Al-Li Conf., G. Champier, B. Dubost, D. Miannay, and L. Sabetay, eds.; *J. Phys.*, 1987, vol. 48, p. C3:891.
9. K.S. Kumar, S.A. Brown, and J.A. Pickens: *Acta Mater.*, 1996, vol. 44, pp. 1899–915.
10. A.K. Gupta, P. Gaunt, and M.C. Chaturvedi: *Phil. Mag.*, 1987, vol. 55, pp. 375–87.
11. M.J. Starink: *Int. Mater. Rev.*, 2004, vol. 49, pp. 191–226.
12. J.M. Papazian, R.N. Deiasi, and P.N. Adler: *Metall. Trans. A*, 1980, vol. 11A, pp. 135–40.
13. J. Karov and W.V. Youdelis: *Mater. Sci. Technol.*, 1986, vol. 2, pp. 681–90.
14. A.K. Jena, A.K. Gupta, and M.C. Chaturvedi: *Acta Metall.*, 1989, vol. 37, pp. 885–95.

15. A.K. Jena, D.P. Lahiri, T.R. Ramachandran, and M.C. Chaturvedi: *J. Mater. Sci.*, 1981, vol. 16, pp. 2544–50.
16. D.J. Lloyd and M.C. Chaturvedi: *J. Mater. Sci.*, 1982, vol. 17, pp. 1819–25.
17. E.S. Balmuth: *Scripta Metall.*, 1984, vol. 18, pp. 301–04.
18. A. Luo, D.J. Lloyd, A. Gupta, and W.V. Youdelis: *Acta Metall. Mater.*, 1993, vol. 41, pp. 769–76.
19. V. Komisarov, M. Tlianker, and B. Cina: *Mater. Sci. Eng.*, 1998, vol. A242, pp. 39–49.
20. K.S. Ghosh, K. Das, and U.K. Chatterjee: *Z. Metallkd.*, 2005, vol. 96, pp. 1404–12.
21. B. Cina: US Patent No. 3,856,584, Dec. 24, 1974.
22. V. Komisarov, M. Tlianker, and B. Cina: *Mater. Sci. Eng.*, 1996, vol. A221, pp. 113–121.
23. M. Kanno, I. Araki, and Q. Cui: *Mater. Sci. Technol.*, 1994, vol. 10, pp. 599–603.
24. A.K. Mukhopadhyay, C.N.J. Tite, H.M. Flower, P.J. Gregson, and F. Sale: *Aluminium-Lithium Alloys*, Proc. 4th Int. Al-Li Conf., G. Champier, B. Dubost, D. Miannay, and L. Sabetay, eds., *J. Phys.*, 1987, vol. 48, p. C3:439.
25. M.J. Starink, A.J. Hobson, and P.J. Gregson: *Scripta Metall.*, 1996, vol. 11, pp. 1711–16.
26. M.J. Starink and P.J. Gregson: *Mater. Sci. Forum*, 1996, vols. 217–222, pp. 673–78.
27. S. Abis, E. Evangelista, P. Mengucci, and G. Riontino: *Aluminium-Lithium Alloys*, Proc. 4th Int. Al-Li Conf., G. Champier, B. Dubost, D. Miannay, and L. Sabetay, eds.; *J. Phys.*, 1987, vol. 48, C3:447.
28. M.C. de Macedo, R.R. Avillez, and I.G. Solorzano: *Scripta Metall.*, 1994, vol. 31, pp. 1701–04.
29. O. Jensrud and N. Ryum: *Mater. Sci. Eng.*, 1984, vol. 64, pp. 229–36.
30. B. Noble and A.J. Trowsdale: *Phil. Mag. A*, 1995, vol. 71, pp. 1345–62.
31. S. Vyazovkin and C.A. Wright: *Int. Rev. Phys. Chem.*, 1998, vol. 17, pp. 407–33.
32. A.K. Galwey and M.E. Brown: in *Handbook of Thermal Analysis and Calorimetry*, M.E. Brown, ed., Elsevier, Amsterdam, 1998, vol. 1, p. 147.
33. J. Sestak, V. Satava, and W.W. Wendlant: *Thermochemica Acta*, 1973, vol. 7, p. 447.
34. H. Himura, R. Kimura, and Hasiguti: *Acta Metall.*, 1962, vol. 10, pp. 607–14.
35. T.L. Koppenaal and M.F. Fine: *J. Appl. Phys.*, 1961, vol. 32, p. 781.
36. C. Wert and C. Zener: *J. Appl. Phys.*, 1950, vol. 5, pp. 21–28.
37. J.M. Silcock: *J. Inst. Met.*, 1960, vol. 89, pp. 203–10.
38. J.W. Christian: *The Theory of Phase Transformation in Metals and Alloys*, 2nd ed., Pergamon Press, Oxford, United Kingdom, 1975, p. 481.
39. M.J. Starink and P.J. Gregson: *Scripta Metall.*, 1995, vol. 33, pp. 893–900.
40. W.S. Miller, L.A. Lennsen, and F.J. Humphreys: *Aluminium Lithium Alloys*, 5th Int. Al- Li Conf., T.H. Sanders, Jr. and E.A. Starke, Jr., eds., MCEP, Williamsburg, VA, 1989, p. 931.
41. B. Noble and G.E. Thompson: *Met. Sci. J.*, 1972, vol. 6, pp. 167–74.
42. S. Caresara, S. Giarda, and A. Sanchez: *Phil. Mag. A*, 1977, vol. 35, pp. 97–110.
43. T. Sato and A. Kamio: *Trans. Jpn. Inst. Met.*, 1990, vol. 29, pp. 25–32.
44. J. del Rio, F. Plazaola, and N. de Diego: *Phil. Mag. A*, 1994, vol. 69, pp. 591–602.